# Journal of Materials Chemistry C

Accepted Manuscript


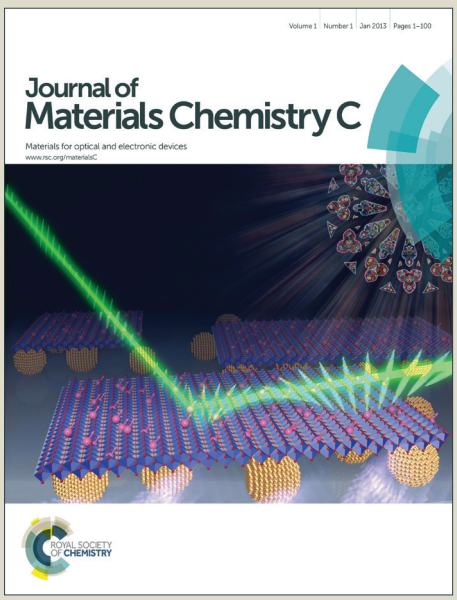





ROYAL SOCIETY OF CHEMISTRY

www.rsc.org/materialsC

Journal Name

RSCPublishing

EDGE ARTICLE

# Covalent Decoration onto the Outer Walls of Double Wall Carbon Nanotubes with Perylenediimides: Synthesis, Characterization and Photoinduced Electron Transfer

Cite this: DOI: 10.1039/xoxxoooooox

Received ooth January 2012,
Accepted ooth January 2012

DOI: 10.1039/xoxxoooooox

www.rsc.org/

Myriam Barrejón,[a] Sara Pla,[b] Isadora Berlanga,††[a] María J. Gómez-Escalonilla,[a] Luis Martín-Gomis,[b] José Luis G. Fierro,[c] Minfang Zhang,[d] Masako Yudasaka,[d] Sumio Iijima,[d] Habtom B. Gobeze,[e] Francis D'Souza,*[e] Ángela Sastre-Santos*[b] and Fernando Langa*[a]

The outer walls of double wall carbon nanotubes (DWCNTs) have been selectively functionalized with different substituted perylenediimides (PDIs) leaving the inner walls intact. The spacer connecting DWCNT and PDI, and the PDI macrocycle position has been varied to visualize the DWCNT-PDI interactions in the hybrids. Evidence of outer wall functionalization and degree of PDI substitution on DWCNT were arrived from HR-TEM, AFM, IR, TGA, XPS and Raman techniques while nanotube-photosentisizer interactions were probed from studies involving optical absorbance and emission, and electrochemical techniques. Fine-tuning of the electronic states of PDI in the hybrids was possible with the present covalent approach. The fluorescence of PDI in the hybrids was found to be quenched (60-70%) due to interactions with DWCNT. Further, femtosecond transient absorption and photocatalytic electron pooling studies were performed to seek evidence of charge separation in these hybrids. In agreement with earlier studies, evidence of charge separation from the transient studies was bleak, and accordingly, yields of photocatalytic electron pooling were much lower than those reported earlier for fullerene and single wall carbon nanotube based hybrids. The present study is suggestive of further tuning of donor-acceptor energy levels in DWCNT derived hybrids for efficient charge separation and stabilization.

*a Instituto de Nanociencia, Nanotecnología y Materiales Moleculares (INAMOL), Universidad de Castilla-La Mancha, 45071-Toledo, Spain. E-mail: Fernando.Langa@uclm.es*
*[b] División de Química Orgánica, Instituto de Bioingeniería, Universidad Miguel Hernández, Avda. de la Universidad, s/n, Elche 03202, Spain. E-mail: asastre@umh.es*
*[c] Instituto de Catálisis y Petroleoquímica, CSIC, Cantoblanco, 28049, Madrid, Spain. E-mail: jlgfierro@icp.csic.es*
*[d] Nanotube Research Center, National Institute of Advanced Industrial Science and Technology,Higashi, Tsukuba, Ibaraki 305-8565, Japan.*
*[e] Department of Chemistry, University of North Texas, 1155 Union Circle, #305070, 76203-5017, Denton, TX, USA. E-mail: Francis.DSouza@UNT.edu*

† Electronic supplementary information (ESI) available: See DOI:
††Current address: Depto. de Física, Universidad de Chile, Av. Encalada 2008, Santiago, Chile.

## Introduction

Carbon nanotubes (CNTs)[1] constitute one of the basic members, together with fullerenes and graphene, of the carbon-based nanomaterials family. Considered as a one dimensional carbon allotrope, CNTs structure can be described as a series of rolled-twisted graphene folders with a high aspect ratio that ranges (i.e. length to diameter radio) from $10^2$ to $10^7$, with remarkable and fascinating properties and enormous potential in technologically strategic areas such electronics, optoelectronics, photovoltaics and sensing applications.[2]

From a structural point of view, CNTs can be characterized by the number of rolled graphene folders. This include tubular structures formed by a unique rolled up graphene folder, the so called single wall carbon nanotubes (SWCNTs), and also multi-wall carbon nanotubes (MWCNTs), which present up to 25 (or more) coaxial CNTs forming a unique cylindrical construction. Thanks to the recently developed technology and technical

efforts, the mass production of structurally homogeneous samples of CNTs has become a reality, thus allowing the systematic investigation on practical technological applications. However, problems do exist for SWCNT to fulfill the high expectations, primarily due to the presence of both metallic and semiconducting tubes regardless of the method of synthesis, and the lack of solubility in most of the commonly used solvents. In most cases, to solubilize SWCNTs, it is desirable to covalently functionalize the $sp^2$ hybridized and fully-conjugated carbon network with electroactive and/or light-absorbing materials, thus causing the disruption of conjugation and therefore, affecting the SWCNT electronic properties.

Double wall carbon nanotubes (DWCNTs) are made of two concentric SWCNTs with an inter-wall spacing of 0.33-0.42 nm,[3] and are emerging as a promising SWCNT substitute as they exhibit higher stability and exhibit improved performance for several applications (e.g., field effect transistors or field emission) compared to SWCNTs.[4] The covalent functionalization of DWCNTs occurs exclusively on the outer wall surface, while the inner tube remains unaltered[5] encouraging a detailed understanding of functionalized-DWCNT electronic properties.

Perylenediimide (PDI) derivatives are a family of dyes that, due to synthetic versatility and easily tunable electronic character,[6] have become one of the most promising classes of molecular materials in organic optoelectronic applications.[7] These systems have been extensively used as electroactive counterpart (either as acceptor or donor moieties) in combination with different carbon nanomaterials, to obtain attractive molecular systems that undergo photoinduced processes.[8] In this context, we recently reported on CNTs (single and multi-wall) covalently functionalized with electron-acceptor PDI derivatives, capable of undergoing photoinduced electron transfer from CNT to perylene appendage, forming the corresponding radical ion pair that persists for about hundred microseconds.[9] However, functionalization of DWCNT with electro-/photoactive molecules, crucial for device applications, has been scarce; only a couple examples involving the covalent linkage of electroactive species to DWCNTs are known[10]; none with PDI derivatives.

In the current study, we focus on three new **DWCNT-PDI** hybrids (Scheme 1) where the electron acceptor ability of PDIs and the mode of linking to the DWCNT have been fine tuned. Besides their synthesis and characterization, their electrochemical and photophysical properties have been studied. Finally, model compounds **PDI 1-3C** have been also synthetized and studied in order to get knowledge on the DWCNT-PDI interactions.

## Results and discussion

The synthesis of the target materials (**DWCNT-PDI 1-3**) was accomplished by covalent anchoring of **PDI 1-3** onto the surface of DWCNTs by using two different approaches: by amidation of previously prepared **DWCNT-COOH** with amino

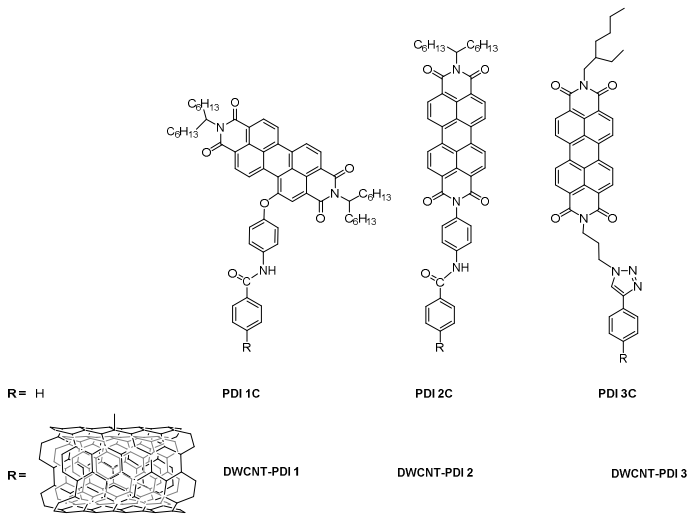


**Scheme 1** New hybrids and reference compounds prepared in this work.

derivatives **PDI 1** and **PDI 2** in the presence of *N,N'*-dicyclohexylcarbodiimide (DCC) and 1- hydroxybenzotriazole (HOBt) to get **DWCNT-PDI 1** and **DWCNT-PDI 2** and via *"click"* chemistry reaction between ethynylphenyl-functionalized DWCNT, (formed by *in situ* removing of the TMS group from **DWCNT-TMS**) and the azide derivative **PDI 3** to obtain **DWCNT-PDI 3** (Scheme 2).

Ultrapure DWCNTs (purity > 98%), stirred in *N*-methyl-2-pyrrolidone (NMP) for 24 h followed by sonication for 6 h were covalently functionalized with: a) $-C_6H_4COOH$ functional groups (**DWCNT-COOH**),[11] by reacting for 24 h at 70 ºC with 4-carboxylbenzenediazonium tetrafluoroborate prepared *in situ* from 4-aminobenzoic acid and isoamyl nitrite, or, b) TMS-protected phenylacetylene (**DWCNT-TMS**) by reaction with 4-(2-trimethylsilyl)ethynyl benzenediazonium tetrafluoroborate under the same conditions (Scheme 2).

On the other hand, the synthesis of **PDI 1** (Scheme 3) was accomplished from aromatic nucleophilic substitution of *N,N'*-di(1-hexyheptyl-1-bromoperylene-3,4,9,10 tetracarboxydiimide[12] with *N*-Boc-4-hydroxyaniline, to obtain **4** in a 60 % yield, followed by *N*-Boc deprotection in the presence of TFA (Scheme 3). $N^1$-(1-hexylheptyl)-$N^2$-(4-aminophenyl)perylene-3,4,9,10-tetracarboxy diimide (**PDI 2**) was prepared following the experimental procedure previously reported.[13] Reference compounds **PDI 1C** and **PDI 2C** were prepared in 65 % and 71 % yield respectively by reaction of **PDI 1** and **PDI 2** with benzoyl chloride (see Scheme 3 and Scheme 4 respectively).

Finally, **PDI 3** was obtained in 24 % yield by condensation of $N^1$-(3-azidopropyl)-3,4,9,10-perylenetetracarboxy-3,4-anhydride-9,10-imide (**5**)[14] with ethylhexylamine in the presence of imidazole (Scheme 5). Reference compound **PDI 3C** was obtained in 60 % yield via copper catalyzed azide-alkynecycloaddition (CuAAC) *"click"* chemistry reaction between **PDI 3** and phenylacetylene. It may be mentioned here

that in the current DWCNT-PDI hybrids, the PDI is almost orthogonal to the DWCNT surface.

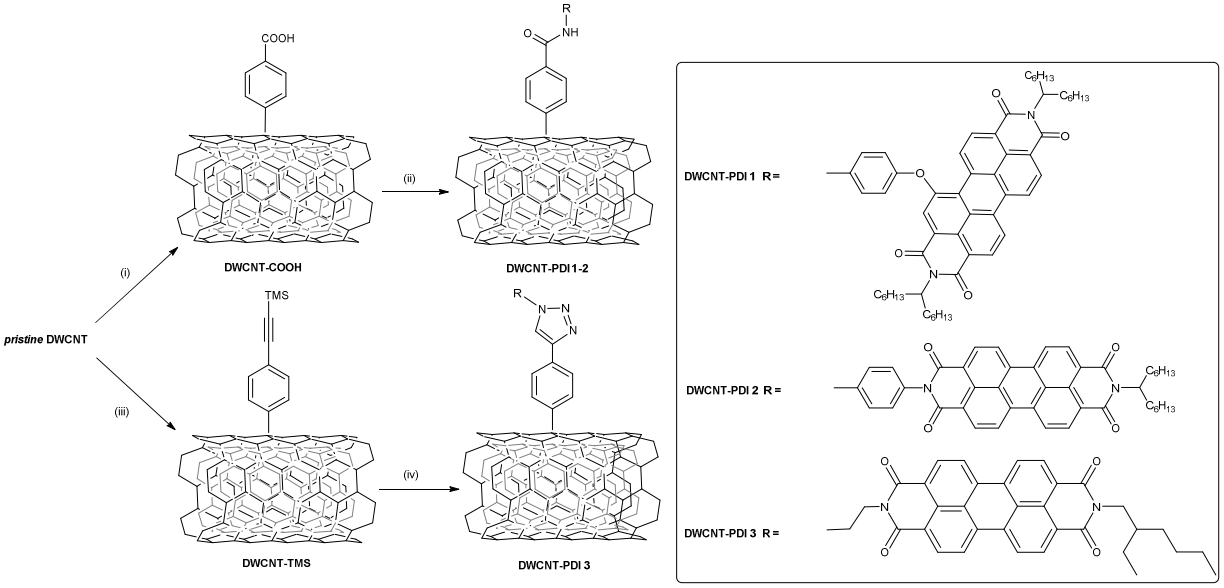


**Scheme 2** Reagents and conditions: (i) 4-aminobenzoic acid, isoamyl nitrite, NMP, 70 °C, 24 h; (ii) **PDI 1** or **PDI 2**, EDC, DMAP, HOBt, NMP, 60°C, 80 h (iii) 4-(2-trimethylsilyl)ethynylaniline, isoamyl nitrite, NMP, 70 °C, 24 h (iv) TBAF, THF/NMP, rt, 1h; then, **PDI 3**, $CuSO_4.5H_2O$, sodium ascorbate, NMP, 70 °C, 48 h.

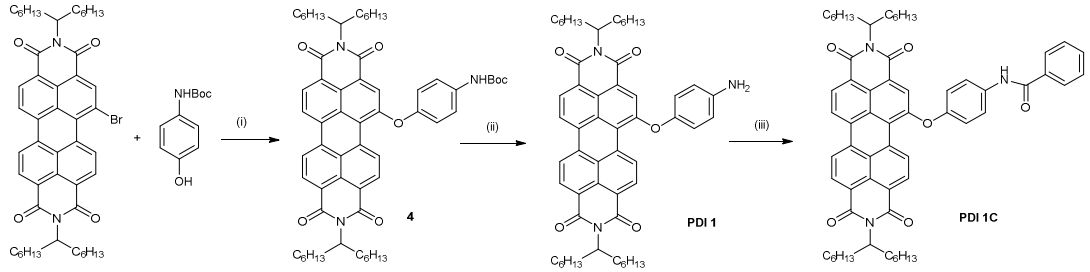


**Scheme 3** Synthesis of **PDI 1** and **PDI 1C**. Reagents and conditions: (i) $K_2CO_3$, 18-Crown-6, Toluene, 80ºC, 5h; (ii) TFA, DCM, 0ºC, 3h; (iii) benzoyl chloride, DCM, rt, 48 h.

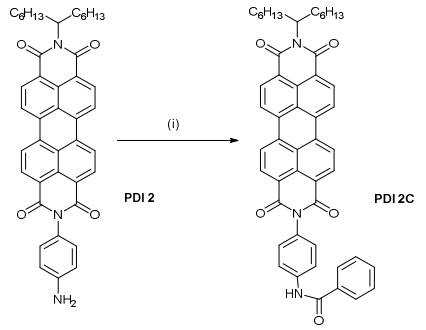


**Scheme 4** Structure of **PDI 2** and synthesis of **PDI 2C**. Reagents and conditions: (i) benzoyl chloride, DCM, rt, 20 h.

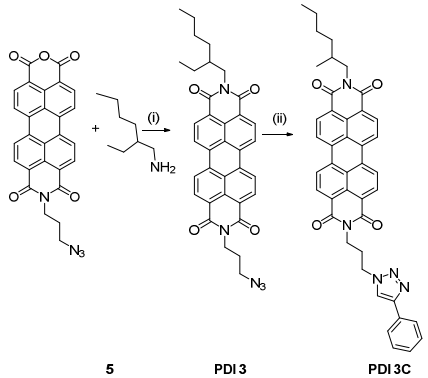


**Scheme 5** Synthesis of **PDI 3** and **PDI 3C**. Reagents and conditions: (i) Imidazole, DMF, 120ºC, 18h. (ii) phenylacetylene, $CuSO_4.5H_2O$, sodium ascorbate, $DCM/H_2O$, rt, 24 h.

All of the new compounds were characterized by common spectroscopic techniques (see ESI†). **DWCNT-PDI 1-3** hybrids were characterized by a full set of analytical techniques, such as thermogravimetric analysis (TGA), Fourier transform infrared spectroscopy (FTIR), atomic force microscopy (AFM), high-resolution transmission electron microscopy (TEM), Raman, X-ray photoelectron spectroscopy (XPS), as well as steady-state and time-resolved spectroscopic techniques.

Evidence of the sidewall functionalization of double wall nanostructures is firstly deduced by comparing the TGA profiles of pristine and functionalized materials. Fig. S25(A-C) (see ESI) shows the thermal behavior of modified DWCNTs (**DWCNT-PDI 1-3**) together with those of their DWCNT precursors (**DWCNT-COOH** or **DWCNT-TMS**) and **PDIs 1-3.** In the 200-600 °C temperature range the thermogram of **DWCNT-COOH** shows a weight loss of 12.72 %. For **DWCNT-PDI 1** an additional weight loss of 8.5 % is observed. Considering that the thermogram of **PDI 1** show an overall descomposition of 55 % at 600 ºC, the actual weight loss due to the attachment of the **PDI 1** is approximately 15.5 %, hence the number of PDIs attached to the sidewall is approximately one group per 499 carbon atoms. With the same calculation, we estimated the actual weight loss for **DWCNT-PDI 2** and **DWCNT-PDI 3** as 16 % and 15 % respectively. As a result, the number of PDIs attached to the sidewall of the nanotubes is one group per 380 carbon atoms for **DWCNT-PDI 2** and one group per 363 carbon atoms for **DWCNT-PDI 3**. [see ESI, Fig. S25(C)].

Raman spectroscopy has proven to be an effective method for DWCNTs characterization.[15] The D band (defect induced mode), almost absent on the pristine sample ($I_D/I_G$ = 0.02), became clear at 1306 $cm^{-1}$ after functionalization by diazonium chemistry ($I_D/I_G$ = 0.07 for **DWCNT-COOH** and $I_D/I_G$ = 0.06 for **DWCNT-TMS**) (Fig. 1). The introduction of disorder into the graphene network by the interaction of aryl moieties with the outer nanotube surface of the outer tube is the origin of this increasing of the $I_D/I_G$ ratio. As expected, the introduction of the perylene groups by amidation (**DWCNT-PDI 1-2**) or *"click"* chemistry (**DWCNT- PDI 3**) does not modify the intensity of the D band. The appearance of a new band at around 1371 $cm^{-1}$ besides the band around 1300 $cm^{-1}$ (that overlaps with D-band) in the final hybrids (**DWCNT- PDI 1-3**), typical of the PDI, demonstrates the presence of the perylene moieties (see Fig. S26).

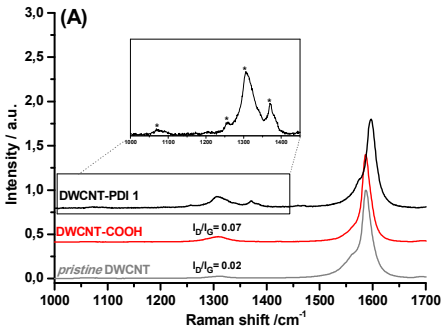


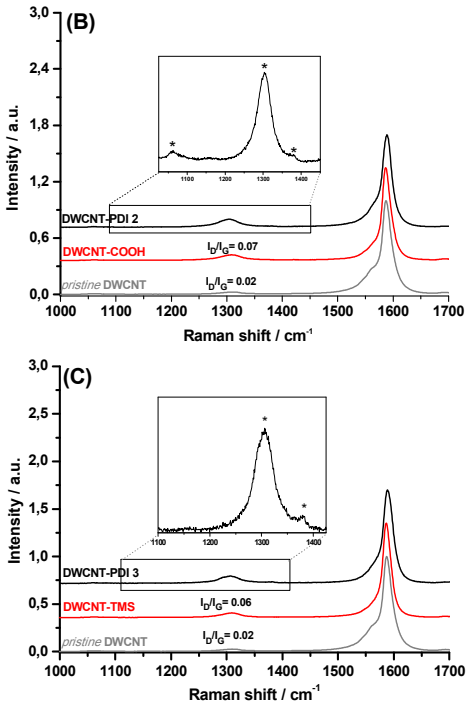


**Fig. 1** Zoom of the Raman spectra of the functionalized **DWCNT-PDIs** series ($\lambda_{exc}$ = 785 nm). In each spectrum, the inset shows the presence of the bands which is attributed of the PDI moieties (*) on the corresponding DWCNT conjugate.

As depicted in Fig. 2, in **DWCNT-PDI 1-3**, the $G^+$ component of the G band is shifted, by 2-9 $cm^{-1}$, to higher wavenumbers respecting to *pristine* DWCNTs due to p-doping[16] effect of the electron-acceptor PDI. The higher shift (9 $cm^{-1}$) observed in **DWCNT-PDI 1** respecting to that in **DWCNT-PDI 2-3** can be related to the parallel orientation of the perylene moiety in **DWCNT-PDI 1**, favouring the π-π interactions.

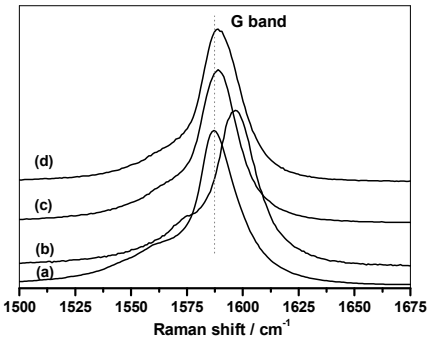


**Fig. 2** G-band region of (a) *pristine* DWCNT sample and functionalized samples (b) **DWCNT-PDI 1**, (c) **DWCNT-PDI 2** and (d) **DWCNT-PDI 3** at 785 nm laser excitation.

Fig. 3 shows the radial breathing modes (RBM) of DWCNTs before and after functionalization by phenylcarboxilyc acid and phenylethynyl group. The diameters of CNTs are related to their RBM frequencies ($\omega_{RBM}$) by the equation ($\omega_{RBM}$) = 218.2/dt + 19.6 $cm^{-1}$, where dt is the diameter of the nanotube (in nm).[17] Thus, the diameters of the outer and inner tubes were found to be ~ 1.00-1.81 nm and ~

0.88 nm respectively. Comparison of the RBM intensity of the inner walls of pristine and functionalized DWCNTs show no significant changes but the lower intensity of the outer walls of functionalized **DWCNT-COOH** and **DWCNT-TMS** respecting to *pristine* DWCNT yields further evidence of the success of functionalization of the outer walls.

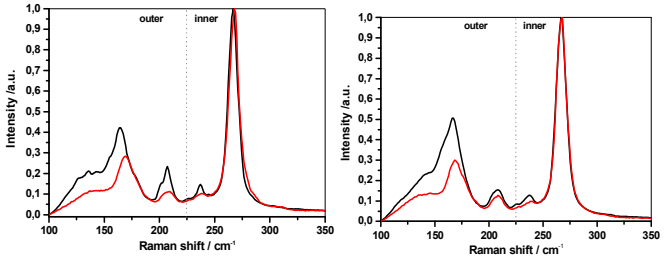


**Fig. 3** RBM zone of: (left) *pristine* DWCNT (black line) and **DWCNT-COOH** (red line); (right) *pristine* DWCNT (black line) and **DWCNT-TMS** (red line) at excitation wavelength of 785 nm.

The FTIR spectroscopy also provides information to the covalent attachment of PDIs to the surface of DWCNTs (see Fig. S28 in ESI). The appearance of the stretching band of the C-H bond in the range of 2848 and 2929 $cm^{-1}$ from the aliphatic part of the PDI moieties is clearly discernible in hybrids **1-3**. Also, as observed in Fig. S28(C), the disappearance of the azide peak at 2096 $cm^{-1}$ of **PDI 3** after the *"click"* coupling confirmed that PDIs units had been covalently bonded to DWCNT through the formation of the triazole ring.[18]

XPS studies also confirmed the functionalization of DWCNTs with PDIs. The binding energies of core levels of the elements of **DWCNT-PDIs 1-3** and the relative proportion of the components of the peaks are collected in Table S1 (see ESI). Also included in this table are the binding energies of the elements of *pristine* DWCNT, **DWCNT-COOH**, **DWCNT-TMS** and **PDIs 1-3** precursors employed in the synthesis of types **DWCNT-PDIs 1-3** structures.

Detailed analysis of the deconvoluted high-resolution C 1s spectrum of the *pristine* DWCNT (see Fig. S29, ESI) showed the main component at 284.8 eV, due the binding energy of the $sp^2$ bonded carbon on the DWCNT surface, and other minor components at 286.2, 287.7 and 289.2 eV assigned to C-O, C=O and COO groups respectively.[19] In addition, a broad small component at about 291.4 eV, originated from the π-π* plasmon emission of C atoms in graphene sheets like structures, was observed.[20] Similarly, the high-resolution O 1s peak of DWCNT has been resolved with two components at 531.8 and 533.3 eV of almost the same intensity. The former component corresponds to O=C bonds and the latter is often associated with O-C[21] bonds demonstrating the existence of both functional groups on the starting DWCNT substrate. Quantitative data in Table 1 indicate that for **DWCNT-COOH** the oxygen increased with respect to *pristine* DWCNT (from 4.9% to 5.7 %), indicating that anchorage of –COOH groups already occurred (see also Fig. S30 in ESI).

Similarly, the anchorage of the **PDI-1** on the **DWCNT-COOH** groups was monitored by XPS. The high resolution C 1s, O 1s and N 1s peaks are displayed in Fig. S31. The C 1s spectrum of **DWCNT-PDI 1** showed substantial differences with respect that of **DWCNT-COOH** sample: (i), the π-π* plasmon component disappeared and (ii), a new component at 285.4 eV assigned to the $sp^3$ carbon atoms, appeared. As this $sp^3$ component comes from alkyl chains, it is inferred that **PDI 1** has been successfully attached on the modified DWCNT substrate. Moreover, the N 1s peak was satisfactorily fitted into two components at 399.2 and 400.3 eV, the intensity of the former being almost twice than the later which are similar to that (399.1 and 400.2 eV, respectively) of the bulk **PDI 1** (see Table S1), indicating that the *N*-bearing groups of the **PDI 1** are present on functionalized DWCNT showing that the amidation reaction between carboxylic acid groups of functionalized DWCNT and terminal $–NH_2$ group of **PDI 1** had occurred. Further support to this conclusion is provided by the 1.5% at of N and the slight increase of O content (8.9 % at) of **DWCNT-PDI 1** with respect its perylene-free **DWCNT-COOH** substrate (Table 1).

**Table 1** Elemental contents of pristine and functionalized DWCNTs

| Sample | Carbon (%at) | Oxigen (%at) | Nitrogen (%at) | Silicon (%at) |
|---|---|---|---|---|
| ***pristine* DWCNT** | 95.1 | 4.9 | - | - |
| **DWCNT-COOH** | 94.3 | 5.7 | - | - |
| **DWCNT-TMS** | 94.5 | 4.8 | - | 0.7 |
| **PDI 1** | 85.3 | 9.6 | 5.1 | - |
| **PDI 2** | 85.3 | 8.5 | 6.1 | - |
| **PDI 3** | 83.1 | 7.5 | 9.4 | - |
| **DWCNT-PDI 1** | 89.6 | 8.9 | 1.5 | - |
| **DWCNT-PDI 2** | 91.4 | 6.8 | 1.8 | - |
| **DWCNT-PDI 3** | 88.3 | 8.1 | 3.6 | - |

In the same way, the C 1s region of **DWCNT-PDI 2** sample (Fig. S32) was fitted into five components: 284.8, 285.3, 286.2, 287.7 and 289.3 eV originated from $sp^2$, $sp^3$, C-O, C=O and COO bonds, respectively. In addition, the N 1s spectrum of **DWCNT-PDI 2** showed two components at binding energies of 399.0 and 400.2 eV, the intensity of the former being about one-half than the later as expected from the structure of **PDI 2**. The similarity of the binding energies of N 1s components together with their relative proportion in functionalized carbon nanotube indicates the introduction of perylene 2 onto the DWCNTs.

Finally, the reaction between **DWCNT-TMS** and **PDI 3** was also followed by photoelectron spectroscopy. The **DWCNT-TMS** substrate showed the same elements of **DWCNT-COOH** sample at almost the same binding energies, together with the Si 2p peak at a BE of 101.5 eV, due to the TMS group (see Fig. S33, ESI). As in the case of previous functionalized DWCNTs, the high resolution C 1s, O 1s and N 1s peaks were fitted with the same components although the respective BEs values and peak areas changed slightly (see Fig. S34). If a comparison is made between the BEs and atomic percentages of the elements in **DWCNT-PDI 3** and **DWCNT-**

**TMS** reference (Table 1), the appearance of N (3.6 % at) and the relative increase in O-content (8.1 %at) with respect **DWCNT-TMS** provide evidence on the success in the click reaction between **PDI 3** and **DWCNT-TMS**.

The morphology of the functionalized hybrids materials **1-3** was observed with TEM and AFM. For example, TEM observation of nanoconjugate **DWCNT-PDI 2** (Fig. 4) showed that the multi-layered structure of nanotubes were not degraded by the chemical processes and there were certain materials attaching to the nanotube wall, which could be perylenediimide moieties.

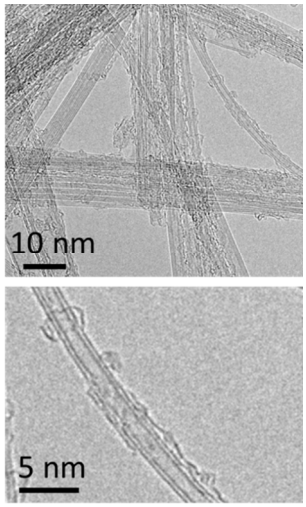


**Fig. 4** Representative TEM image of **DWCNT-PDI 2** hybrid material.

The diameter of the nanoconjugates **DWCNT-PDI 1-3** were measured by Atomic Force Microscopy (AFM). The analysis of *pristine* DWCNT resulted on a diameter distribution in the range of 1-3 nm with average diameter of ~ 2 nm (see ESI, Fig. S35). In the case of hybrid **1**, as shown in Fig. 5, after incorporation of **PDI 1** on the surface of double wall carbon nanotube, the average diameters found is 3.2+1 nm (based on a statistics of 125 nanotubes). According to these measurements, covalently attached perylenediimide addend generates an average increase of around 1.9-2.5 nm. The estimated length of the PDI moiety **1** (1.9-2.5nm) was estimated from the more stable conformations obtained by means of molecular mechanics; so, the observed increase fits quite well with that expected for these hybrid. Additionally, very thin bundles or individual tubes can be seen at the edges corresponding to non-functionalized DWCNTs (Fig. 5 (b) height profiles A and D).

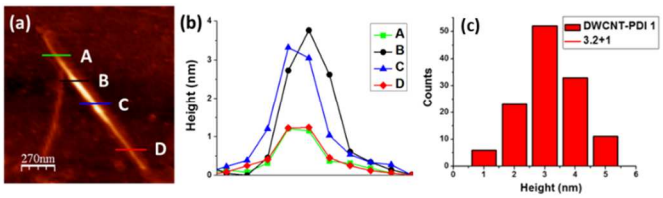


**Fig. 5** (a) AFM image of **DWCNT-PDI 1** on a mica substrate, (b) the Z-profiles indicated with lines A, B, C and D are shown in the graph, and (c) diameter distribution histogram of the hybrid **1**.

The electrochemical behaviour of **DWCNT-PDIs** and reference compounds **PDI 1-3C** has been investigated by cyclic voltammetry (CV) and Osteryoung Square Wave Voltammetry (OSWV) at room temperature in a standard three-electrode cell, in dry o-DCB/acetonitrile 4:1 solution containing 0.1 M tetrabutylammonium hexafluorophosphate ($TBAPF_6$) as supporting electrolyte. Comparison between the reduction potential of **DWCNT-PDIs** and their respective reference compounds **PDICs** give light on the electronic interactions between the carbon nanotube and the PDI. Results are shown in Table 2 and Fig. S36.

Reference perylenediimides **PDI 1-3C** are active in the cathodic zone showing two reduction potentials in the observation window. **PDI 2C** show a lower first reduction potential, by 40-50 mV, than the other two PDI derivatives as result of its better electron acceptor ability. Comparison of the first reduction potential of the hybrids and reference compounds show, in all cases, small shifts to more negative values when the PDIs are covalently attached to the DWCNTs respecting to the reference compounds, evidencing electronic communication between both electroactive groups, the electron donor CNT and the electron acceptor PDI. It may be mentioned here that during anodic excursion of potential, no sharp peak corresponding to oxidation of DWCNT was observed, although the currents were higher than the background currents. This could be due to the presence of DWCNT of different sizes revealing anodic process in a range of potential rather than at a fixed value.

**Table 2** Electrochemical data [V *vs* Fc/Fc+] for the reduction process of functionalized DWCNTs and its reference compounds (**PDI 1-3C**) determined by OSWV.[a]

| Compound | $E_{red}^1$(V) | $E_{red}^2$(V) |
|---|---|---|
| **PDI 1C** | -1.13 | -1.33 |
| **DWCNT-PDI 1** | -1.15 | -1.36 |
| **PDI 2C** | -1.07 | -1.30 |
| **DWCNT-PDI 2** | -1.10 | -1.27 |
| **PDI 3C** | -1.14 | -1.26 |
| **DWCNT-PDI 3** | -1.20[b] | |

[a] In *o*-DCB/acetonitrile 4:1 solution (0.1 M $TBAPF_6$) at room temperature. [b] Broad reduction peak due to the overlapping of the first and second reduction processes.

The ground-state features of perylendiimides in the final nanohybrids were probed by steady-state absorption experiments (Fig. 6 and S37). The UV-vis spectra of functionalized **DWCNTs** were recorded in comparison with its control perylendiimides **PDI 1-3C** in benzonitrile (PhCN) and NMP as solvents. In hybrids **2** and **3**, we observe a small red-shift in the absorption maxima corresponding to the PDI chromophore (450-550 nm), when compared with that its PDIs references see Fig. S37 (B) and (C))], suggesting again the existence of electronic interactions between DWCNTs and PDIs in the ground state; this shift is higher when the spectra were recorded in NMP ($E_T$(30) NMP = 42.2 kcal/mol versus

$E_T(30)$ PhCN = 41.5 kcal/mol). Nevertheless, the most interesting feature in the absorption spectra of **DWCNT-PDI** hybrids is the appearance of a new band at around 550 nm; this band is more clearly observed in hybrids **DWCNT-PDI 2-3** (Fig. 6) where the degree of functionalization is higher. To determine the origin for this band, the absorption spectra of **DWCNT-PDI 2-3** were registered in solvents of different polarity as chlorobenzene ($E_T(30)$ = 36.8 kcal/mol) and NMP ($E_T(30)$ NMP = 42.2 kcal/mol). Whilst the absorption bands corresponding to the PDI chromophore were shifted by 2-3 nm when the more polar NMP was used as solvent, respecting to chlorobenzene, the shift of the new band was higher (4-7 nm, see Figure 6) indicating higher influence of solvent's polarity and suggesting the existence of charge transfer. To confirm this hypothesis, a mixture of DWCNT and PDI-3C was prepared; the absorption spectrum of the mixture (just prepared) did not show the presence of this band, but it can be observed after 5 h. (Figure S42) indicating a dynamic process, which can be assigned to charge transfer.

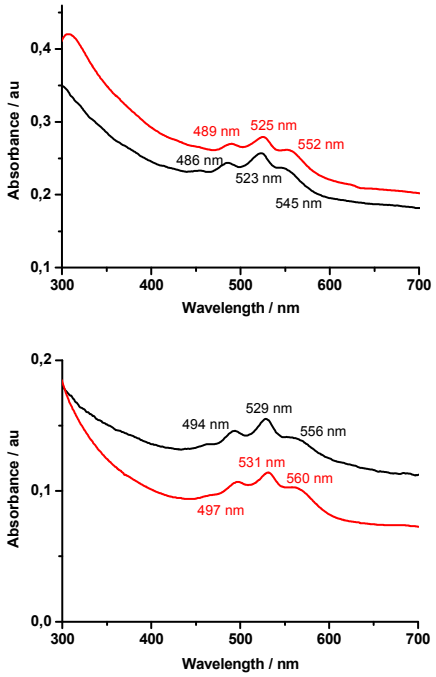


**Fig 6**. Absorption spectra of: (upper part) **DWCNT-PDI 2** in chlorobenzene (black line) and NMP (red line) as solvents. (Lower part) **DWCNT-PDI 3** in chlorobenzene (black line) and NMP (red line) as solvents.

The existence of electronic interactions between PDI moieties and DWCNTs is also supported by emission spectroscopy by comparing the fluorescence of reference compounds **PDI 1-3C** with the fluorescence observed for **DWCNT- PDI 1-3** when excited at the maximum absorption wavelength of PDICs. In all cases (see Fig. 7), the fluorescence of PDI in the hybrids is weaker than those of the reference compounds (~ 60-70%) indicating that DWCNTs quench the emission of the attached PDI. These results suggest existence of nonfluorescent static complex in the hybrids (via intra- or intermolecular association) or occurrence of electron transfer from DWCNT to the singlet excited PDI.

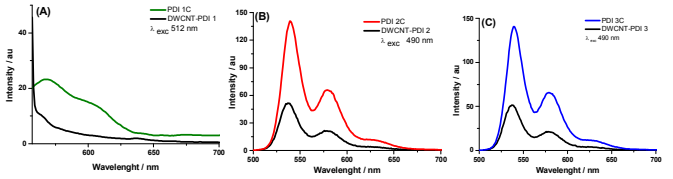


**Fig. 7** Fluorescence spectra of **DWCNT-PDIs** hybrid materials (black line) as compared with its control **PDIs** ((A) 1 (—), (B) 2 (—) and (C) 3 (—)), obtained in NMP as solvent. The excitation wavelength was indicated in each case, and the concentrations were adjusted showing the same optical density at the excitation wavelength.

Further, femtosecond transient absorption and electron pooling studies were performed to secure evidence for any electron transfer in these donor-acceptor hybrids. First, photoluminescence behaviour of *pristine* DWCNT utilized in the present study was examined in SDBS micellar solution since better exfoliation of nanotubes compared to that in organic solvents is generally observed in this media.[24] As shown in Fig. S38, although weak, DWCNTs in SBDS solution revealed weak emission bands whose peak positions matched those of SWCNTs. Earlier, Weisman and co-workers[25a] attributed this to the presence of small percentage of SWCNTs trapped in commercial samples of DWCNTs, such as the one used in the present study, and that the DWCNTs are non-luminescent with very low quantum yields.[25b] TEM images in Fig. 4 clearly shows large majority of the tubes to be DWCNTs with trace amounts of SWCNTs, often stacked with the DWCNTs.

Transient absorption studies on perylenediimide precursors used to derivatise DWCNTs were performed in Ar-saturated NMP. As shown in Fig. 8 and Fig. S39 in ESI, at the excitation wavelength of 400 nm, transient spectra revealed negative peaks in the 485, 528 and 580 nm range, opposite mimic of the ground state absorption and positive peaks in the 650-1000 nm range with peak maxima at 700 nm. The ground state recovery of the 528 nm band and decay of the 700 nm band (see Fig. 7c and d) for all three cases appeared to be mirror images. It may be mentioned here that in the case of **DWCNT-PDI 1** and **DWCNT-PDI 2**, the singlet decay was complete within 100-200 ps, suggesting additional intramolecular events. It is known that the one-electron reduced product of perylenediimide, $PDI^{-}$ exhibits absorption bands close to $^1$PDI* in the 700 nm range.[26] A close examination of the spectra in Fig. 8 and Fig. S39, decay of the 700 nm band was accompanied by a relatively broad peak in the 720 nm range, suggesting that the strong electron acceptor, PDI might be involved in excited state electron transfer with nitrogen bearing functional groups on the macrocycle periphery (see Scheme 1 for structures) or the NMP solvent.[27]

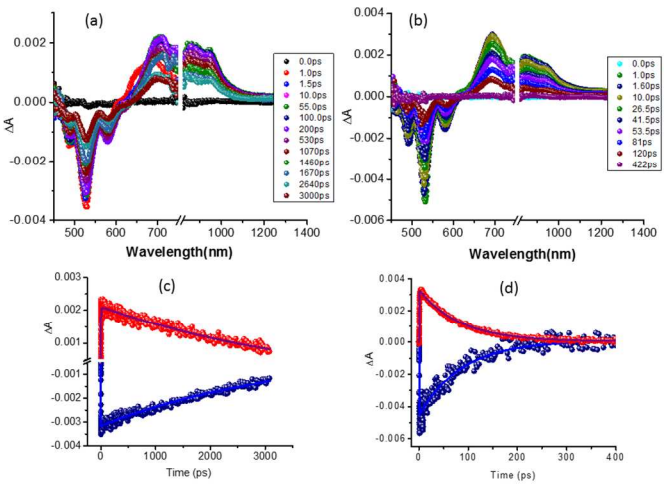


**Fig. 8** Femtosecond transient spectra of (a) **PDI 3C** and (b) **PDI 2C** in Ar- saturated NMP at the excitation wavelength of 400 nm at the indicated time intervals. Figures c and d show the time profiles of the 528 and 700 nm bands of the respective PDI derivatives.

Fig. 9a and b show the transient absorption spectra of **DWCNT-PDI 3** and **DWCNT-PDI 2** hybrids while Fig. S40 in ESI provides the spectra of **DWCNT-PDI 1** hybrid in NMP. Immediately after excitation, strong exciton bands both in the visible and near-IR region within 1 ps were observed. At 1 ps, peak minima at 518, 551, 700, 1004, 1089, 1200 and 1337 nm were observed irrespective of the nature of the hybrids. These peak positions matched that of *pristine* SWCNTs and the total recovery of these bands occurred within 3-4 ps (Fig. 8c and d, and Fig. S40b), time constant reported earlier for SWCNT exciton recovery.[28] At higher time scales of over 4 ps, no new peaks corresponding to either $^{1}$PDI* or PDI$^{-}$ or DWCNT$^{+}$ suggesting that the time scale for all these processes are much smaller and that any signal corresponding to these processes are buried within the exciton peaks originated from trace amounts of SWCNTs in the sample. Alternatively, this could also suggest lack of electron transfer in the DWCNT-PDI hybrids as another possibility.

Studies on the utilization of donor-acceptor nanohybrids as a photocatalysts to accumulate electron transfer products is highly useful not only to gather additional evidence of electron transfer in the nanohybrids especially when the spectroscopic evidence of electron transfer is bleak but also as functional materials for light driven catalytic processes such as solar fuel production.[29] In this regard, one of the well-established methods in our laboratory involves photocatalytic electron pooling using methyl viologen ($MV^{2+}$) as an electron acceptor, and 1-benzyl-1,4-dihydronicotinamide (BNAH) as a sacrificial electron donor.[30,31] By repeated irradiation, using a Xe lamp with a 400 nm filter to excite sensitizer selectively and not the additives ($MV^{2+}$ and BNAH), accumulation of $MV^{+}$ could be monitored at 608 nm. We have successfully employed this strategy to probe photocatalytic behavior of donor (sensitizer)-fullerene and donor (sensitizer)-SWCNT derived donor-acceptor hybrids.[31] In the present study, we have extended the electron pooling experiments to probe electron transfer, if any, in the nanohybrids.

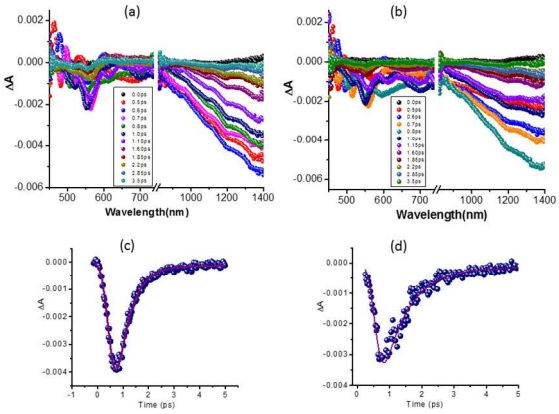


**Fig. 9** Femtosecond transient spectra of (a) **DWCNT-PDI 3** and (b) **DWCNT-PDI 2** in Ar-saturated NMP at the excitation wavelength of 400 nm at the indicated time intervals. Figs. c and d show the time profile of the 1200 nm peak attributed to exciton of trace amounts of SWCNT present in the sample.

Fig. 10a shows the spectrum of **DWCNT-PDI 1** in the presence of $MV^{2+}$ and various amounts of BNAH. Similar spectra were obtained for other investigated hybrid systems. It could be seen that in the absence of BNAH, when the concentration of $MV^{2+}$ is 0.5 mM in the hybrid solution, no peak at 608 nm corresponding to the formation of $MV^{\cdot+}$ was observed. However, $MV^{\cdot+}$ peak appears in the presence of BNAH which increase with the increase in concentration of BNAH. This suggests that the BNAH acts as a sacrificial hole-shifting component in the electron mediation experiment.[30,31] As depicted in Fig. S41 in ESI, the photocatalytic process involves electron pooling into the added $MV^{2+}$ in the presence of hole shifter BNAH by the continuous irradiation of the nanohybrids. Control experiments were also performed by utilizing perylene precursors without DWCNTs under similar experiments conditions. As shown in Fig. 10b, efficiency of electron pooling for the donor-acceptor hybrids is at least twice as much as that of pristine perylenediimide precursors highlighting the importance of having both donor and acceptor in the photocatalytic cycle. However, the overall electron pooling efficiencies for DWCNT-PDI hybrids are much lower than that reported for fullerene or SWCNT based hybrids,[31] indicating poor electron transfer efficiencies (including contributions from the trace amounts of SWCNT hybrids), as suggested by fluorescence and transient absorption studies. It may be mentioned here that in a study by Aurisicchio and co-workers,[32] the authors concluded lack of electron transfer in porphyrin-DWCNT hybrid materials wherein the utilized porphyrin was an electron donor unlike the electron acceptor, PDI used in the present study. These studies suggest DWCNT being a poor electron donor and poor electron acceptor in hybrid systems.

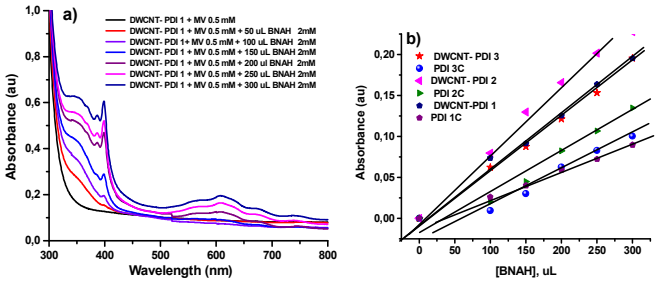


**Fig. 10** (a) Electron pooling experiment of PDI-DWCNT hybrids dissolved in DMF containing 0.5 mM $MV^{2+}$ upon addition of increasing amounts of BNAH. (b) Extent of $MV^{\cdot+}$ formation for the hybrids and control compounds revealing the effect of DWCNT in improving electron pooling ability.

## Conclusions

Three different DWCNT-PDI covalent hybrids were synthesised and fully characterized by TEM, AFM, IR, TGA, XPS and Raman, showing functionalization of the outer wall leaving the inner walls intact. The optical absorbance and fluorescence, and electrochemical studies were performed and compared with those of their reference compounds, without carbon nanotubes, to visualize PDI-DWCNT interactions. Such comparison showed electronic communication between the two active species, and the possibility of DWCNT acting as electron donor and the PDI acting as electron acceptor in the hybrid. However, evidence of photoinduced electron transfer from DWCNT to the singlet excited PDI from the femtosecond transient absorption and photocatalytic electron pooling studies were rather weak warranting additional tuning of energy levels in the hybrid. Currently, such studies are in progress in our laboratories to accomplish efficient charge separation in DWCNT derived donor-acceptor hybrids as light energy harvesting nanomaterials.

## Experimental section

### Synthesis of functionalized DWCNT-PDIs

### General procedure for the preparation of DWCNT-PDI 1 and 2

**DWCNT-COOH** (4 mg) was dispersed in NMP (20 mL) and subsequently added to a stirred solution of the corresponding perylenediimide (10 mg), DCC (1 equiv), dimethylaminopyridine (DMAP) (1 equiv) and 1-hydroxybenzotriazole (HOBt) (1.2 equiv). The resulting mixture was stirred for 60 h at 60 ºC. The crude was then filtered on a PTFE membrane and washed with methanol and dichloromethane to afford the desired material.

### Synthesis of DWCNT- PDI 1

According to the general procedure, **DWCNT-COOH** (4 mg), **PDI 1** (10 mg, 0.012 mmol), DCC (2.5 mg, 0.012 mmol), DMAP (1.5 mg, 0.012 mmol) and HOBt (1.9 mg, 0.014 mmol) in NMP (20 mL) gave the desired product (7 mg).

### Synthesis of DWCNT-PDI 2

According to the general procedure, **DWCNT-COOH** (4 mg), **PDI 2** (10 mg, 0.015 mmol), DCC (3.1 mg, 0.015 mmol), DMAP (1.9 mg, 0.015 mmol) and HOBt (2.4 mg, 0.018 mmol) in NMP (20 mL) gave the desired product (6 mg).

### Deprotection of DWCNT-TMS

To a suspension of **DWCNT-TMS** (15 mg) in NMP (50 mL) at 0ºC was added a solution of tetrabutylammonium fluoride (TBAF) (1M in THF) (2mL). The reaction mixture was stirred at room temperature for 2 h and then filtered on a PTFE membrane (0.2 µm). The nanotubes were washed several times with NMP and then with dichloromethane, redissolved in NMP and used directly for the next step.

### Synthesis of DWCNT-PDI 3

To a suspension of deprotected **DWCNT-TMS** (10mL) in NMP (40mL) were added **PDI 3** (25 mg, 0.043 mmol), $CuSO_4.5H_2O$ (11 mg, 0.043 mmol) and sodium ascorbate (8.5 mg, 0.043 mmol). The reaction mixture was stirred at 70°C for 48 h and then filtered on a PTFE membrane (0.2 µm). In order to remove sodium ascorbate, copper catalyst and free perylene, the black solid was washed with NMP and then with dichloromethane yielding the desired material (17 mg).

## Acknowledgments

This research was financially supported by the Spanish Ministry of Economy and Competitiveness (Mineco) of Spain (CTQ2013-48252-P and CTQ2011-26455), Junta de Comunidades de Castilla-La Mancha (PEII-2014-014-P), Generalitat Valenciana (PROMETEO 2012/010 and ISIC/2012/008) and the US-National Science Foundation (Grant No. 1401188 to FD). One of us (MB) thank a FPI grant from Mineco.

## References

1 (a) S. Iijima, *Nature*, 1991, **354**, 56–58; (b) S. Iijima and T. Ichihashi, *Nature*, 1993, **363**, 603–605.

2 (a) G. S. Tulevski, A. D. Franklin, D. Frank, J. M. Lobez, Q. Cao, H. Park, A. Afzali, S.-J. Han, J. B. Hannon and W Haensch, *ACS Nano,* 2014, **8**, 8730–8745; (b) F. Cicoira, C. M. Aguirre and R. Martel, *ACS Nano,* 2011, **5**, 283-290; (c) K. Dirian, M. A. Herranz, G. Katsukis, J. Malig, L. Rodríguez-Pérez, C. Romero-Nieto, V. Strauss, N. Martín and D. M. Guldi, *Chem. Sci*., 2013, **4**, 4335-4353.

3 Y. Li, K. Wang, J. Wei, Z. Gu, Z. Wang, J. Luo and D. Wu, *Carbon,* 2005, **43**, 31-35.

4 M. Kalbac, A. A. Green, M. C. Hersam and L. Kavan, *ACS Nano,* 2010, **4**, 459-469.

5 (a) H. Muramatsu, Y. A. Kim, T. Hayashi, M. Endo, A. Yonemoto, H. Arikai, F. Okino and H. Touhara, *Chem. Commun*., 2005, 2002 -2004; (b) G. Marcolongo, G. Ruaro, M. Gobbo and M. Meneghetti, *Chem. Commun*., 2007, 4925 - 4927; (c) J. F. Colomer, R. Marega, H. Traboulsi, M. Meneghetti, G. van Tendeloo and D. Bonifazi, *Chem. Mater*.,

2009, **21**, 4747 -4749; (d) T. Hayashi, D. Shimamoto, Y. A. Kim, H. Muramatsu, F. Okino, H. Touhara, T. Shimada, Y. Miyauchi, S. Maruyama, M. Terrones, M. S. Dresselhaus and M. Endo, *ACS Nano,* 2008, **2**, 485-488; (e) L. G. Bulusheva, A. V. Okotrub, E. Flahaut, I. P. Asanov, P. N. Gevko, V. O. Koroteev, Yu. V. Fedoseeva, A. Yaya and C. P. Ewels, *Chem. Mater.,* 2012, **24**, 2708-2715.

6 (a) F. Würthner, *Chem. Commun*., 2004, 1564-1579; (b) H. Langhals, *Helv. Chim. Acta*, 2005, **88**, 1309-1343.

7 (a) C. Huang, S. Barlow and S. R. Marder, *J. Org. Chem*., 2011, **76**, 2386–2407; (b) C. Li and H. Wonneberger, *Adv. Mater*., 2012, **24**, 613-636; (c) E. Kozma and M. Catellani, *Dye. Pigment.*, 2013, **98**, 160-179; (d) M. Guide, S. Pla, A. Sharenko, P. Zalar, F. Fernández-Lázaro, Á. Sastre-Santos and T.-Q. Nguyen, *Phys. Chem. Chem. Phys*., 2013, **15**, 18894-18899; (e) Q. Yan, Y. Zhou, Y.-Q. Zheng, J. Pei and D. Zhao, *Chem. Sci*., 2013, **4**, 4389-4394; (f) X. Zhang, Z. Lu, L. Ye, C. Zhan, J. Hou, S. Zhang, B. Jiang, Y. Zhao, J. Huang, S. Zhang, Y. Liu, Q. Shi, Y. Liu and J. Yao, *Adv. Mater*., 2013, **25**, 5791–5797; (g) R. Shivanna, S. Shoaee, S. Dimitrov, S. K. Kandappa, S. Rajaram, J. R. Durrant and K. S. Narayan, *Energy Environ. Sci*., 2014, **7**, 435–441.

8 (a) R. Gómez, J. L. Segura and N. Martín, *Org. Lett*., 2005, **7**, 717–720; (b) P. Dyad, Y. Shibano, T. Umeyama, Y. Matano, N. V. Tkachenko, H. Lemmetyinen and H. Imahori, *Org. Lett*., 2006, **8**, 4425–4428; (c) J. Baffreau, S. Leroy-Lhez, V. A. Nguyên, R. M. Williams and P. Hudhomme, *Chem. Eur. J*., 2008, **14**, 4974–92; (d) T. W. Chamberlain, E. S. Davies, A. N. Khlobystov and N. R. Champness, *Chem. Eur. J*., 2011, **17**, 3759–3767; (e) U. Hahn, J.-F. Nierengarten, B. Delavaux-Nicot, F. Monti, C. Chiorboli and N. Armaroli, *New J. Chem*., 2011, **35**, 2234-2244; (f) L. Feng, M. Rudolf, S. Wolfrum, A. Troeger, Z. Slanina, T. Akasaka, S. Nagase, N. Martín, T. Ameri, C. J. Brabec and D. M. Guldi, *J. Am. Chem. Soc*., 2012, **134**, 12190–12197; (g) R. K. Dubey, M. Niemi, K. Kaunisto, A. Efimov, N. V Tkachenko and H. Lemmetyinen, *Chem. Eur. J*., 2013, **19**, 6791–6806; (h) S. Pla, L. Martín-Gomis, K. Ohkubo, S. Fukuzumi, F. Fernández-Lázaro and Á. Sastre-Santos, *Asian J. Org. Chem*., 2014, **3**, 185–197.

9 R. Martín, F. J. Céspedes-Guirao, M. de Miguel, F. Fernández-Lázaro, H. García and Á. Sastre-Santos, *Chem. Sci*., 2012, **3**, 470–475.

10 (a) M. Vizuete, M. J. Gómez-Escalonilla, S. García-Rodríguez, J. L. García Fierro, P. Atienzar, H. García and F. Langa, *Chem. Eur. J*., 2012, **18**, 16922-16930; (b) M. Vizuete, M. J. Gómez-Escalonilla, J. L. García Fierro, P. Atienzar, H. García and F. Langa, *ChemPhysChem*, 2014, **15**, 100–108.

11 J. Huang, A. L. Ng, Y. Piao, C.-F. Chen, A. A. Green, C.-F. Sun, M. C. Hersam, C. S. Lee and Y. H. Wang, *J. Am. Chem. Soc*., 2013, **135**, 2306−2312.

12 H. Langhals and S. Kirner, *Eur. J. Org. Chem*., 2000, **2000**, 365–380.

13 M. Wolffs, N. Delsuc, D. Veldman, N. V. Anh, R. M. Williams, S. C. J. Meskers, R. A. J. Janssen, I. Huc and A. P. H. J. Schenning, *J. Am. Chem. Soc*., 2009, **131**, 4819-4829.

14 H. J. Kitto, E. Schwartz, M. Nijemeisland, M. Koepf, J. J. L. M. Cornelissen, A. E. Rowan and R. J. M. Nolte, *J. Mater. Chem*., 2008, **18**, 5615-5624.

15 C. Shen, H. Brozena and Y. Wang, *Nanoscale,* 2011, **3**, 503-518.

16 (a) R.Voggu, C. S. Rout, A. D. Franklin, T. S. Fisher and C. N. R. Rao, *J. Phys. Chem. C*, 2008, **112**, 13053-13056; (b) G. M. Do Nascimento, T.Hou, Y. A. Kim, H. Muramatsu, T. Hayashi, M. Endo, N. Akuzawa and M. S. Dresselhaus, *Carbon*, 2011, **49**, 3585–3596.

17 A.A. Green and M. C. Hersam, *ACS Nano*, 2011, **5**, 1459-1467.

18 (a) M. Vizuete, M. J. Gómez-Escalonilla, J. L. G. Fierro, M. Yudasaka, S. Iijima, M. Vartanian, J. Iehl, J.-F. Nierengarten and F. Langa, *Chem. Commun*., 2011, **47**, 12771–12773; (b) M. Barrejón, M. Vizuete, M. J. Gómez-Escalonilla, J. L. G. Fierro, I. Berlanga, F. Zamora, G. Abellán, P. Atienzar, J.-F. Nierengarten, H. García and F. Langa, *Chem. Commun*., 2014, **50**, 9053–9055.

19 E. Bekyarova, M. E. Itkis, P. Ramesh, C. Berger, M. Sprinkle, W. A de Heer and R. C. Haddon, *J. Am. Chem. Soc.*, 2009, **131**, 1336–7.

20 S. Utsumi , H. Honda , Y. Hattori , H. Kanoh , K. Takahashi , H. Sakai , M. Abe, M. Yudasaka , S. Iijima and K. Kaneko, *J. Phys. Chem. C*, 2007, **111**, 5572–5575.

21 A. Jung, R. Graupner, L. Ley and A. Hirsch, *Phys. Status Solidi*, 2006, **243**, 3217–3220.

22 (a) E. E. Neuteboom, E. H. A. Beckers, S. C. J. Meskers, E. W. Meijer and R. A. J. Janssen, *Org. Biomol. Chem*., 2003, **1**, 198-203; (b) F. Würthner and A. Sautter, *Org. Biomol. Chem*., 2003, **1**, 240-243; (c) T. V. D. Boom, R. T. Hayes, Y. Zhao, P. J. Bushard, E. A. Weiss and M.R. Wasielewski, *J. Am. Chem. Soc.*, 2002, **124**, 9582-9590.

23 M. Supur, Y.Yamada, M. E. El-Khouly, T. Honda and S. Fukuzumi, *J. Phys. Chem. C,* 2011, **115**, 15040–15047.

24 D. A. Tsyboulski, J.-D. R. Rocha, S. M. Bachilo, L. Cognet and R. B. Weisman, *Nano Lett.,* 2007, **7**, 3080-3085.

25 (a) D. A. Tsyboulski, Y. Hou, N. Fakhri, S. Ghosh, R. Zhang, S. M. Bachilo, M. Pasquali, L. Chen, J. Li and R. B. Weisman, *Nano Lett.*, 2009, **9**, 3282-3289; (b) T. Koyama, Y. Asada, N. Hikosaka, Y. Miyata, H. Shinohara and A. Nakamura, *ACS Nano,* 2011, **5**, 5881-5887.

26 M. T. Vagnini, A. L. Smeigh, J. D. Blakemore, S.W. Eaton, N. D. Schley, F. D'Souza, R. H. Crabtree, G. W. Brudvig, D. T. Co and M. R. Wasielewski, *Proc. Natl. Acad. Sci*., 2012, **109**, 15651-15656.

27 B. A. Ruzicka, R. Wang, J. Lohrman, S. Ren and H. Zhao, *Phys. Rev. B*, 2012, **86**, 205417.

28 Y. Shibono, T. Umeyama, Y. Matano, N. V. Tkachenko, H. Lemmetyinen and H. Imahori, *Org. Lett*., 2006, **8**, 4425-4428.

29 F. D'Souza and O. Ito, *Chem. Soc. Rev*., 2012, **41**, 86-96.

30 S. Fukuzumi, H. Imahori, K. Ohkubo, H. Yamada, M. Fujitsuka, O. Ito and D. M. Guldi, *J. Phys. Chem. A*, 2002, **106**, 1903-1908.

31 F. D'Souza, A. S. D. Sandanayaka and O. Ito, *J. Phys. Chem. Letts.,* 2010, **1**, 2586-2593.



 

32 C. Aurisicchio, R. Marega, V. Corvaglia, J. Mohanraj, R. Delamare, D. A. Vlad, C. Kusko, C. A. Dutu, A. Minoia, G. Deshayes, O. Coulembier, S. Melinte, Ph. Dubois, R. Lazzaroni, N. Armaroli and D. Bonifazi, *Adv. Funct. Mater*., 2012, **22**, 3209-3222.

Table of contents

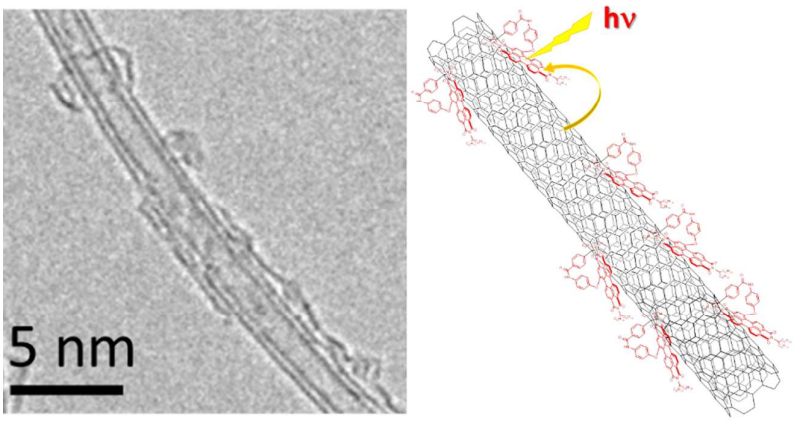


Three new covalently bonded double wall carbon nanotube-perylenediimide nanohybrids (DWCNT-PDIs) have been synthesized and characterized, showing exclusively functionalization of the carbon nanotube outer wall leaving the inner walls intact. Absorbance, emission and electrochemical studies show electronic communication between the two active species. Femtosecond transient absorption and photocatalytic electron pooling studies were performed to seek evidence of charge separation in these hybrids.